Large Diurnal Heating of the Sea Surface Observed by the HCMR Experiment

P. Y. DESCHAMPS[1] AND R. FROUIN[2]

Laboratoire d'Optique Atmosphérique, Equipe associée au CNRS n° 466, Université des Sciences et Techniques de Lille, 59655 Villeneuve d'Ascq cédex, France

(Manuscript received 25 May 1982, in final form 31 August 1983)

ABSTRACT

Day–night surface temperature differences measured in the infrared (10.5–12.5 μm channel) by the HCMR satellite experiment frequently show large diurnal heating (several °C) of the upper layer of the ocean during the summer months in the Mediterranean Sea when the wind speed is low. When observed in the 0.5–1.1 μm channel, glitter reflectance—i.e., direct solar radiation specularly reflected towards the sensor—correlates with diurnal heating. Glitter reflectance has been modeled to retrieve an equivalent wind speed. Observed diurnal heatings (ΔT) do not exceed 5°C, in agreement with the limit value calculated from the heat transfer equation assuming thermal diffusivity is only molecular. The influence of wind speed can be approximately described by $\Delta T = 0.4U^{-1} + 0.5$ (in °C for U in m s^{-1}), for U less than 2 m s^{-1}. A mean diurnal heating of nearly 1°C is calculated for the marine coastal areas of southern France. During this period, satellite observations should be restricted to night and early morning orbits, or to periods of high wind speed ($U > 5$ m s^{-1}).

1. Introduction

A daily variation in the temperature of the surface layer of the oceans is known to be produced by diurnal heating due to absorbed solar radiation. The amplitude of the daily temperature variation is usually small because of turbulent mixing which usually prevails over the molecular thermal diffusivity. A solar irradiance of 1000 W m^{-2}, when absorbed in a mixed layer of 10 m, would give a heating rate of only 0.1°C h^{-1}, and a daily variation of less than 0.5°C. If the turbulent mixing is reduced and the mixed layer is less than 1 m thick, a heating rate of 1°C h^{-1} may be expected and daily variations of several °C should be observed. With the exception of very shallow waters, large diurnal surface temperature variations in open oceans correspond to low wind speeds because turbulence in the surface layer is mainly induced by the surface wind stress.

From a theoretical simulation of radiative and heat transfer in the upper ocean, Hasse (1971) predicted that the deviation of the sea surface temperature (SST) T_0 from the bulk temperature T_{10} taken at 10 m depth should vary as:

$$T_0 - T_{10} = C_1 Q U^{-1}, \qquad (1)$$

where Q is the solar irradiance, U the wind speed and $C_1 = 3.5 \times 10^{-3}$ when Q is expressed in W m^{-2} and U in m s^{-1}. According to Hasse, Eq. (1) is only valid for $U > 2$ m s^{-1}, but the evidence that the SST diurnal variations increase when U decreases is supported by several observations: Romer (1969), Stommel *et al.* (1969) occasionally found diurnal variations of more than 1°C at very low wind speeds—i.e., for $U < 2$ m s^{-1}. These observations were nevertheless restricted to a single location and were isolated events.

Satellite infrared radiometers offer the opportunity to more systematically investigate such diurnal variations of the SST. The first satellite experiment to provide adequate capability for this purpose was the Heat Capacity Mapping Radiometer (HCMR) experiment launched in late April 1978 with an improved temperature resolution (0.3°C) and a nearly noon overpass. Results from this experiment are hereby reported in order 1) to investigate large diurnal SST variations at low wind speeds and 2) to give an assessment of the relative frequency of such an event and its impact on the determination of the SST field in such areas as the Mediterranean Sea where diurnal heating is frequent.

2. Observations of diurnal heating from HCMR satellite data

a. The HCMR experiment

The basic objective of the HCMR experiment is the measurement of variations of the Earth surface temperature for applications to Earth resources (geology, hydrology, etc.). For this purpose, the satellite is sun-synchronous and crosses the equator at about 0200 and 1400 local time so that surface temperature data

[1] Present affiliation: Centre National d'Etudes Spatiales, 18 Avenue Edouard Bélin, 31055 Toulouse, France.

[2] Present affiliation: California Space Institute, A-021, Scripps Institution of Oceanography, La Jolla, CA 92093.

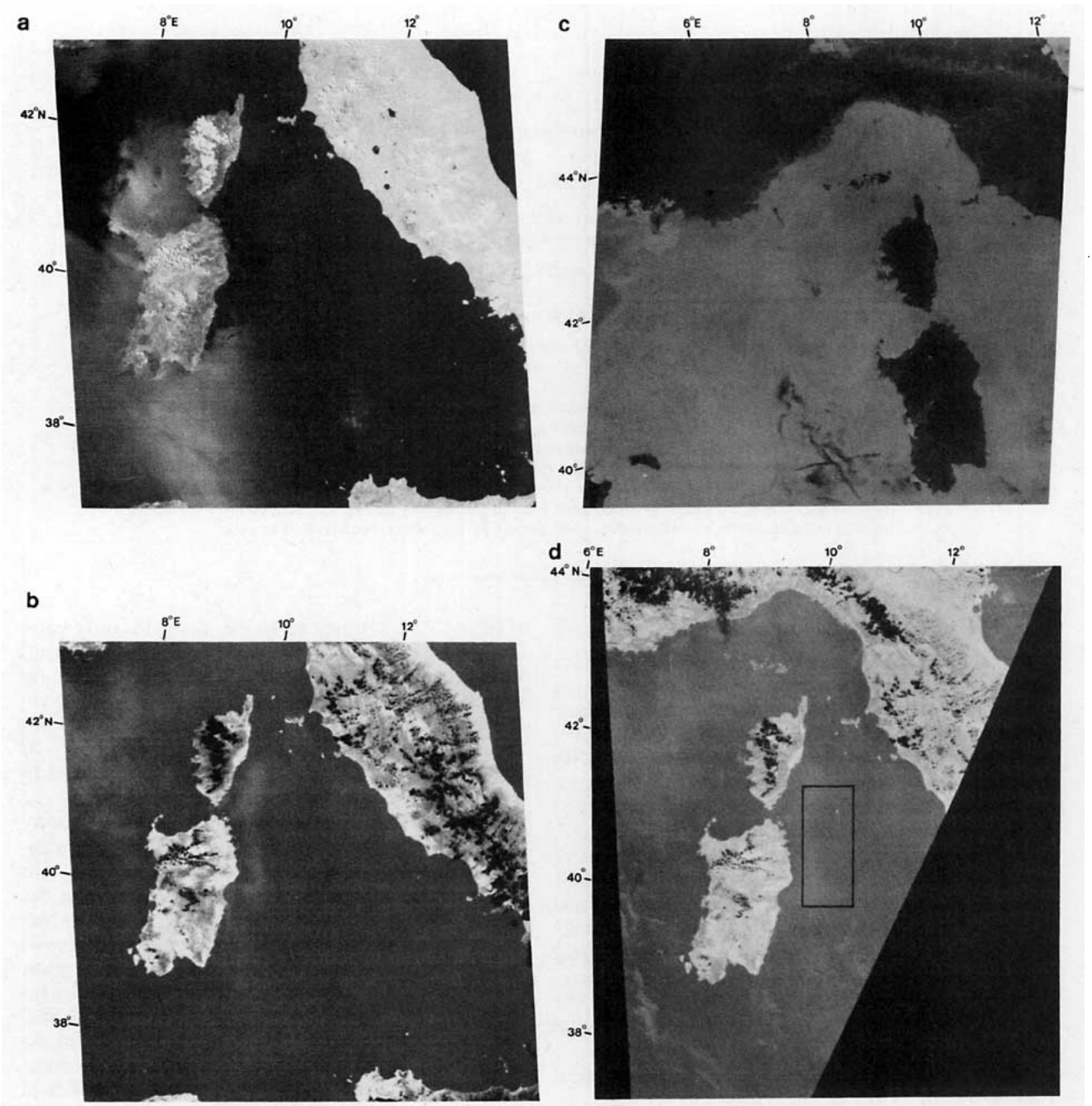

FIG. 1. Diurnal heating in the Western Mediterranean Sea: (a) Day HCMR scene A-A0038-12440 at 1244 GMT 3 June 1978. Image center is at 40.54°N, 011.04°E. Visible channel: darker tones are lower reflectances. Note the bright patterns east and west of Corsica and Sardinia. (b) Same as (a) but for infrared channel: darker tones are colder surface temperatures. Note warmer waters east and west of Corsica and Sardinia. (c) Night HCMR scene A-A0038-01490 at 0149 GMT 3 June 1978. Infrared channel: darker tones are colder temperatures. (d) Day-night temperature differences between HCMR scenes obtained at 0149 (night) and 1244 GMT (day) 3 June 1978. Darker tones are smaller diurnal heatings. Study area is indicated by a rectangle. (e) Meteorological situation at 1200 GMT 3 June 1978.

are obtained close to the minimum and the maximum of the diurnal variation. Satellite altitude is 620 km, and orbit inclination is 98.87°. The HCMR consists of a two-channel scanning/imaging radiometer, with a 0.5–1.1 μm spectral bandwidth in the visible and 10.5–12.5 μm in the thermal infrared. Similar channels have been used on previous meteorological satellites, but the interests of the HCMR experiment are 1) a large improvement of the radiometric performances in the thermal infrared channel: temperature resolution

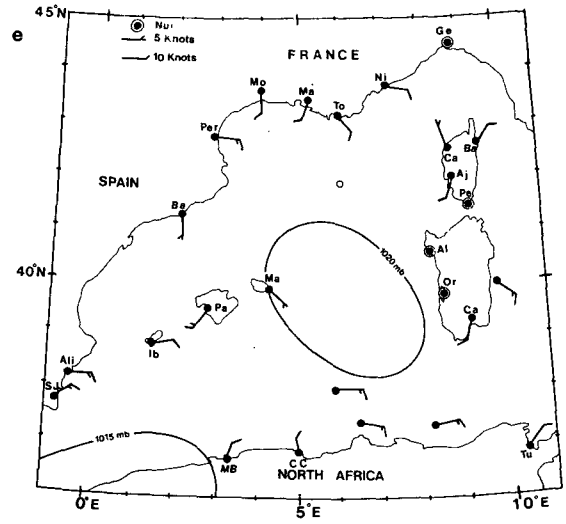

FIG. 1. (*Continued*)

of 0.3°C and nadir ground resolution of 500 m as compared with 0.5–1°C and 1 km for the previous VHRR (Very High Resolution Radiometer) experiment on NOAA satellites, 2) the new ease with which the user can obtain differential surface temperature maps between day and night at 12 or 36 hour intervals. The HCMR experiment was originally designed to produce thermal inertia data for soil and geology applications but the very good performances of HCMR are also suitable for oceanographic studies. Data were received from NASA (National Aeronautics and Space Administration) through an investigation concerned with sea surface temperatures of the coastal zones of France.

Available HCMR data are photographic or digital products covering a 700 × 700 km^2 scene. The following information is displayed: 1) diffuse surface albedo or reflectance in the visible channel (day only), 2) surface temperature from the infrared channel, 3) surface temperature difference between day and night and 4) thermal inertia, which was not used in the present study. About 1000 photographic products covering the coastal zones of France were received during the May 1978–May 1979 period. Examples of the photographic products are given for two areas in the Western Mediterranean Sea (Fig. 1) and in the North Sea (Fig. 2) where large diurnal variations of the SST were observed.

b. Diurnal heating and glitter (sun glint) patterns

A large number of the imagery derived from data received for the Mediterranean Sea during May, June and July 1978 exhibited very interesting and concordant features in both the visible and the infrared channels. These are shown in Fig. 1, for the waters between the Island of Corsica and the Southern coast of France, and also close to the East coasts of Corsica and Sardinia. In these instances, the warmer areas in the thermal imagery are often associated with brightness changes in the visible imagery.

The observed brightness changes in the visible are glitter or sunglint patterns, i.e., specular reflection of direct solar radiation by the wavy sea surface. The time period of this study is around the summer solstice and the observation angle of the HCMR imagery is very close to the angle of the specular reflection of direct solar radiation in the Western part of the scenes. This favors the observation of glitter patterns. Glitter generally increases when the wind decreases and the sea surface becomes calmer and more specular. The surface exhibits a maximum brightness when the observation angle is close to that of the specular reflection of solar radiation: a homogeneous bright area is thus noted in the southwest part of Fig. 2b. For very calm seas, the surface reflection becomes nearly specular, and a brightness decrease may be observed because it is very unlikely that the observation angle be strictly in line with the specular reflection. Both processes are present in the northwest part of Fig. 1a, where bright and dark areas respectively correspond to weak and nul wind speeds. The fact that smoothing of the surface could produce either an increase or a decrease of the glitter brightness was previously mentioned by La Violette *et al.* (1980). A physical and detailed description is given in the Appendix, to aid in a further quantitative analysis of the data. The dark patterns in a mean bright glitter can thus be clearly interpreted as nul wind and thus, calm sea areas. Such an area would obviously favor greater diurnal heating of the upper layer of the ocean because the transfer of heat to the deeper ocean layers is limited by reduced turbulent mixing and thermal diffusivity.

c. Meteorological observations

Evidence of a large diurnal heating corresponding to low wind speed conditions is also given by correlative meteorological observations. Surface observations are presented in Fig. 1e for the case of the Mediterranean Sea, and in Fig. 2d for another case found in the North Sea for which, due to unfavorable geometry conditions of observation, the visible imagery (Fig. 2a) does not show the presence of sunglint patterns. On Fig. 2b a large warm spot was detected by HCMR in the middle of the North Sea which was coincident with the center of an anticyclone high where nul wind speed was reported. Warmer areas observed in the Mediterranean Sea on Fig. 1b are also coincident with low or nul wind speeds. However, the observed wind field is complicated by the coastal weather station reports being biased by coastal effects superimposed upon the anticyclone high. Cloud free satellite SST observations are frequently acquired during similar anticyclone situations with moderate wind speeds. It must be stressed

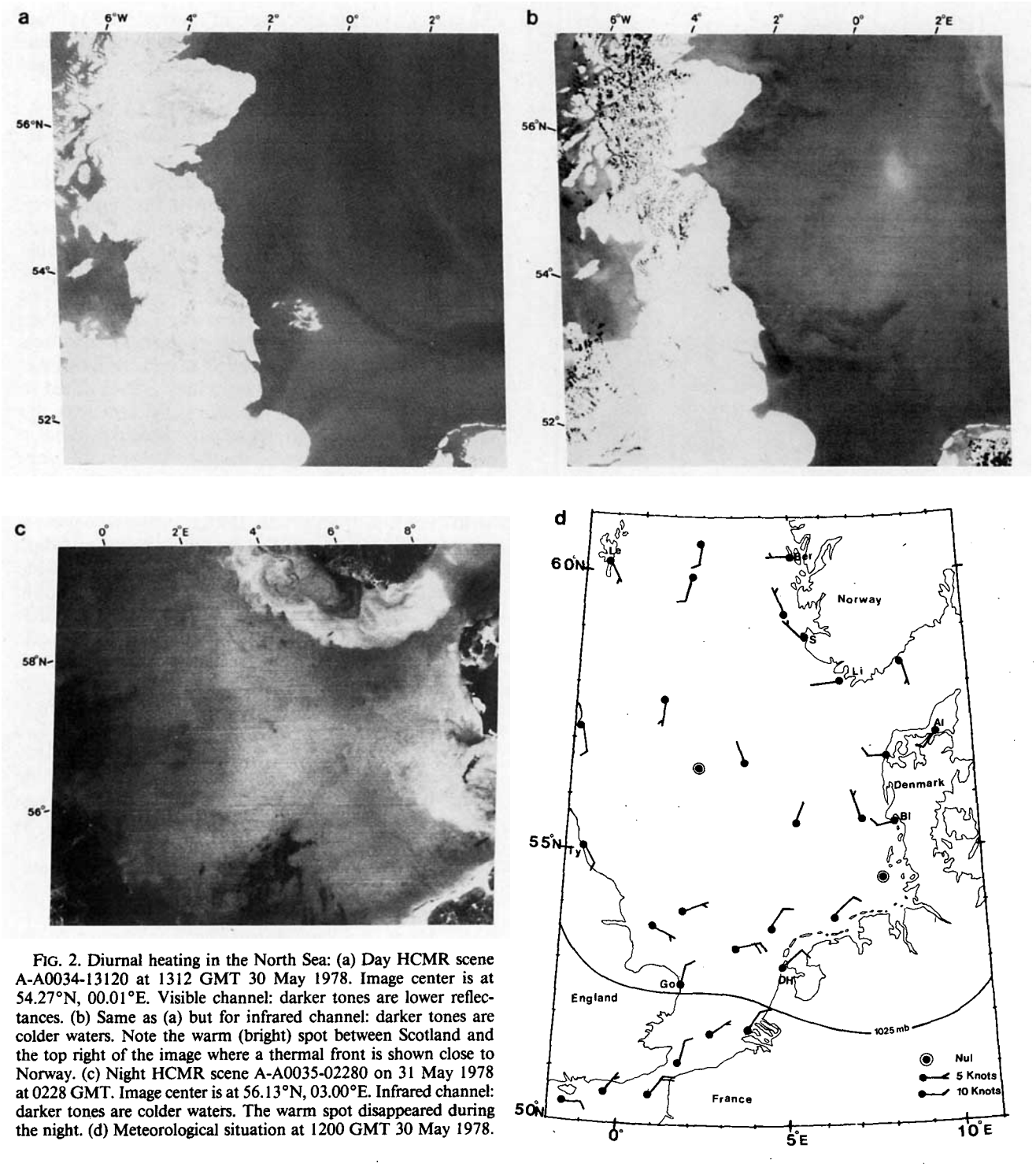

FIG. 2. Diurnal heating in the North Sea: (a) Day HCMR scene A-A0034-13120 at 1312 GMT 30 May 1978. Image center is at 54.27°N, 00.01°E. Visible channel: darker tones are lower reflectances. (b) Same as (a) but for infrared channel: darker tones are colder waters. Note the warm (bright) spot between Scotland and the top right of the image where a thermal front is shown close to Norway. (c) Night HCMR scene A-A0035-02280 on 31 May 1978 at 0228 GMT. Image center is at 56.13°N, 03.00°E. Infrared channel: darker tones are colder waters. The warm spot disappeared during the night. (d) Meteorological situation at 1200 GMT 30 May 1978.

that satellite estimations of SST may thus be systematically affected by diurnal heating, and a tentative statement of this is discussed in Section 3d.

d. Day–night observations

In the upper layers of the ocean, heat loss during the night very rapidly destroys most of the heating produced during the day. Evidence of diurnal heating may thus be found from a comparative analysis of consecutive day and night observations 12 h apart. For the two cases given in Figs. 1b and 2b, the corresponding night observations (Figs. 1c and 2c) show a much more constant SST field and the warmer features noted during day time disappear.

Figure 1d gives the result of the computed day–night temperature differences after the proper calibration algorithms have been applied by NASA. These differences present the advantage of being independent of the mean mesoscale SST field and allow enhancement of the diurnal heating, which again closely correlates with glitter patterns in the visible channel. Day–night temperature differences are used in the following or a more quantitative analysis of diurnal heating.

3. Dependence of diurnal heating on sea state and wind speed

The observed diurnal heatings were further quantified by analysis to derive their relationship with the sea state and the wind speed. Day–night temperature differences were correlated to the reflectance of the 0.5–1.1 μm channel. This reflectance, mostly due to sun glitter, is related to the surface slope variance and to a mean wind speed using the statistical model of Cox and Munk (1954).

a. Diurnal heating and glitter reflectance

Day–night temperature differences (Fig. 1d)—i.e., SST diurnal variations—show patterns similar to the glitter patterns (Fig. 1a), on 3 June 1978. Fig. 3 gives the result of the correlation obtained when the diurnal heating ΔT is plotted as a function of the glitter reflectance ρ_g in a small study area East of Sardinia (Fig. 1d). It is evident that a close correlation exists and ΔT rapidly decreases when ρ_g increases. To further interpret that fact, ρ_g has to be related to the wind speed, or, more exactly, to the statistics of surface slopes.

Using the statistical distribution of surface slopes from Cox and Munk (1956), a model was developed to relate the glitter reflectance to the wind speed. This model is detailed in the Appendix. Results indicate that ρ_g could either increase or decrease with wind speed: ρ_g presents a maximum value for a given wind speed value, both of which depend on solar and observation angles through θ_n ($\tan\theta_n$ is the surface slope allowing specular reflection towards the sensor). Fig. 4 gives the relationship between ρ_g and the wind speed U for θ_n = 8, 10 and 12°, corresponding to the area previously studied for $\Delta T = f(\rho_g)$. In this case ρ_g increases rapidly at the lower wind speeds and then is rather constant for $U > 3$ m s^{-1} so that U can be estimated with a good accuracy from ρ_g, only when $U < 3$ m s^{-1}. The study has thus to be limited to this wind speed range. It is important to note that ρ_g is physically linked to the surface slope variance, and only statistically to the wind speed. Local anomalies may thus occur, in particular when the fetch of the wind over the sea is variable. Keeping these precautions in mind, we may now transform $\Delta T(\rho_g)$ into $\Delta T(U)$ which is given in Fig. 5.

b. Diurnal heating and the wind speed

The first point to be noted on Fig. 5, which gives the diurnal heating as a function of the wind speed, is that T rapidly decreases from several to 1°C when U increases up to 2 m s^{-1}. The scatter of observations $\Delta T(U)$ on Fig. 5 is remarkably less than $\Delta T(\rho_g)$ on Fig. 3 because the variations of ρ_g with changes of observation angles within the study area have been eliminated. A fit of $\Delta T(U)$ would give:

$$\Delta T = 0.4U^{-1} + 0.5 \quad [\text{°C for } U \text{ in m s}^{-1}]. \quad (2)$$

Some uncertainties related to the model $\rho_g(U)$ have been previously outlined. Additional errors may be due to atmospheric effects on the measured radiances. An aerosol atmospheric reflectance of 0.02 was estimated from the minimum reflectance within the scene ($\rho_g \approx 0$) and substracted in the 0.5—1.1 μm channel.

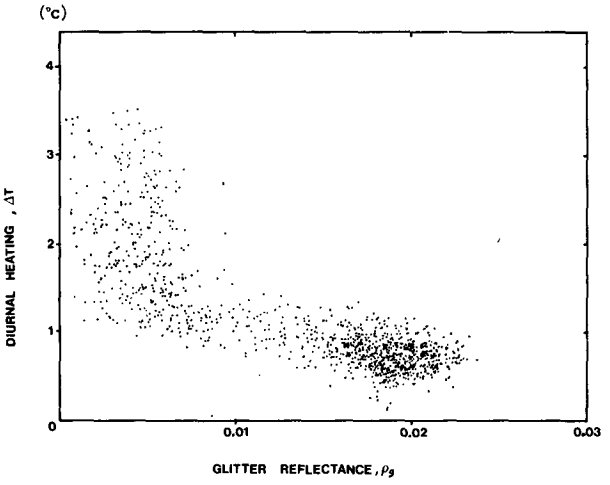

FIG. 3. Day-night temperature difference vs glitter reflectance on 3 June 1978, for the study area East of Sardinia.

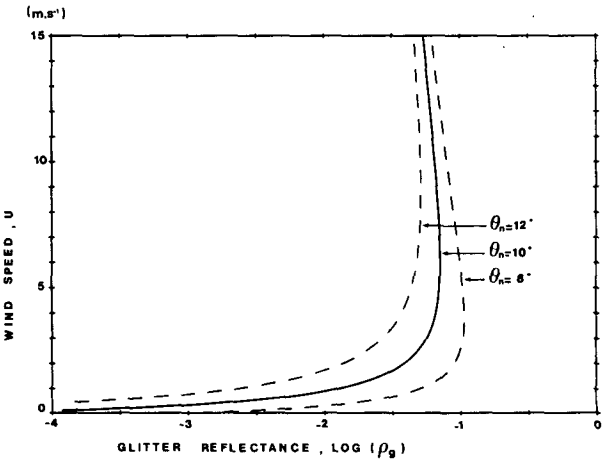

FIG. 4. Retrieved wind speed vs glitter reflectance for the study area.

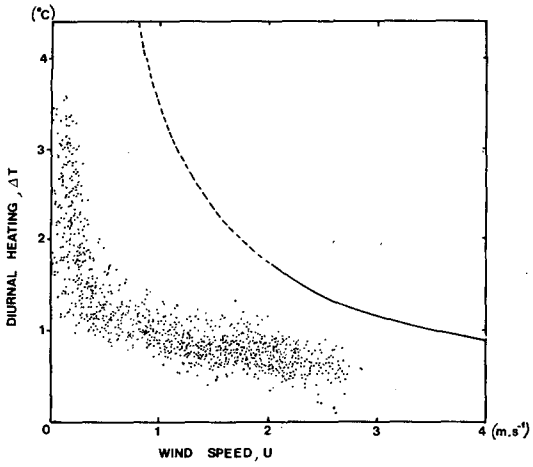

FIG. 5. Day-night temperature difference vs retrieved wind speed for the study area. The solid-dashed line shows the diurnal heating obtained from Hasse (1971), which is valid only for $U > 2$ m s^{-1}.

Day–night temperature differences have not been corrected for atmospheric emission in the infrared. Consequently, the observed ΔT are certainly underestimated by a factor τ, the atmospheric transmittance in the 0.5–1.1 μm band, which typically equals 0.7 for a midlatitude summer atmosphere. In addition, a bias due to a change of atmospheric parameters (temperature, water vapor concentration) could have occurred between day and night observations which would possibly explain the 0.5°C constant found in (2). Typical diurnal changes of air temperature and relative humidity near the surface are 1.5°C and 4% respectively in midlatitude marine regions during summer (Roll, 1965), and can account for the observed bias.

The results may be compared to the values predicted by Hasse (1971). Using in (1) a mean solar irradiance at sea level $Q = 900$ W m^{-2}, ΔT is found to vary as $1.5U^{-1}$. This relationship is shown in Fig. 5 and when compared to HCMR observations, gives a systematic overestimation of the diurnal heating for $U < 3$ m s^{-1}. Moreover, the Hasse curve does not reach a limit value of ΔT when $U = 0$. As pointed out by Hasse, the results of the model given in (1) cannot be applied to the lower wind speed range because the model refers to a steady state assumption not respected by scales of a few hours.

c. *Limit value of the diurnal heating*

Figure 5 and other HCMR scenes with large diurnal heatings indicate that diurnal heatings do not exceed about 5°C, and that a limit value should exist at low wind speed. This value may be obtained by solving the heat transfer equation

$$\frac{d}{dz}\left[k(z)\frac{dT(z,t)}{dt}\right] + \frac{dF(z,t)}{dz} = \rho c \frac{dT(z,t)}{dt} \quad (3)$$

for $k(z) = k_m$, the thermal conductivity of sea water—i.e., no turbulent diffusivity is assumed at $U = 0$. Eq. (3) was solved using the conditions

$$F(z, t) = F(0, t)g(z) - F_0, \quad (4)$$

where $F(0, t)$ is the solar irradiance at sea level and F_0 the heat loss by the surface, and

$$g(z) = a_i \exp(-k_i z), \quad (5)$$

where a_i, k_i are given in Table 1 and were obtained from a fit of $g(z)$ according to the work by Pruvost (1975). In (4), $g(z)$ is considered independent of time. This is a rather good approximation since the underwater penetration of direct solar radiation is close to nadir even at low solar elevation angles. As pointed out by Simpson and Dickey (1981), the influence of water clarity on penetrating solar irradiance may lead to significantly different upper ocean temperatures, particularly at low wind speeds, and must be taken in account in downward irradiance parameterization. The irradiance constants listed in Table 1 are valid for clear waters [type 1 and 2 waters in Jerlov (1968) classification], which is likely the case in the study area. A homogeneous layer is assumed to exist just below the surface. The depth z_0 of this layer is defined similarly to the model of Kraus and Turner (1967): the variation of potential energy produced by solar radiation and surface heat loss is equal to the work of the wind stress on the sea surface, i.e. nul for this study case where we look for a limit value of ΔT at $U = 0$. Under these conditions, ΔT variance correlates well with the net heat budget of the surface

$$\Delta T \approx C \int_0^{t_0} (F(0, t) - F_0)dt, \quad (6)$$

where $C = 0.65 \times 10^{-6}$ °C J^{-1} m^2. For the HCMR observations on 3 June 1978

$$\frac{1}{t_0}\int_0^{t_0} (F(0, t) - F_0)dt$$

is estimated to be a mean value of 600 W m^{-2} over a period of 4 h (in fact a maximum value of 900 W m^{-2} at noon, the time of satellite overpass), and we find

$$\Delta T = 5.6°\text{C}. \quad (7)$$

TABLE 1. Coefficients a_i, k_i in (5) for water penetration by solar irradiance.

i	a_i	k_i (m^{-1})
1	0.041	3365.9
2	0.139	201.18
3	0.211	13.05
4	0.24	1.22
5	0.37	0.07

This value is in agreement with the observations reported in Fig. 5. At the lower wind speed, the observed diurnal heating is widely scattered within the range of $2 < \Delta T < 4$°C, and thus below the estimated limit value. The large variations of the observed ΔT at $U \approx 0$ may be explained by the fact that Eq. (6) requires a nul wind speed during the entire heating period preceeding the observation, i.e., several hours, which is very unlikely. The scatter of the diurnal heating at $U \approx 0$ therefore is probably linked to time variations of the local wind speed.

d. *Frequency of diurnal heating*

From 13 May to 28 August 1978, 60 HCMR synoptic measurements taken over the Western Mediterranean Sea were examined of which ~34 measurements exhibited large (typically more than 1°C) diurnal heating of particular areas of 10 to 100 km width. Relative frequency of the event is rather large, and is enhanced in some areas affected by a shore breeze and where the wind systematically becomes nul at some distance from the coast. Table 2 gives relative frequencies of low wind speeds ($U < 3$ m s^{-1}) at some stations along the coast of France during the summer months (from Darchen, 1974). The frequency of nul wind allowing a diurnal heating of more than 1°C is between 10 and 30%. The frequency of low wind speed ($1 < U < 3$ m s^{-1}) varies from 20 to 50%, allowing a diurnal heating of about 1°C. From these frequencies, N_1 and N_2, a mean diurnal heating $\bar{\Delta}T$ was calculated as

$$\bar{\Delta}T = 2.5N_1 + N_2 \tag{8}$$

and is also given in Table 2. The mean diurnal heating ranges from 0.5 to 1.5°C along the south coast of France with a maximum on the French Riviera (Cap Ferrat).

4. Conclusion

The present investigation, using SST satellite observations from the HCMR experiment has shown a high frequency of large diurnal heatings (more than 1°C) of the sea surface during summer months in such areas as the Mediterranean Sea where low wind speeds are very frequent. This shows that satellite observations made at noon and during the afternoon should be checked to eliminate those corresponding to low wind speed ($U < 3$ m s^{-1}). If not, a systematic bias could be introduced in the SST analysis of some areas, particularly the marine coastal areas affected by a sea–land breeze effect.

Using simultaneous observations of the glitter reflectance, the diurnal heating was correlated to the wind speed. Diurnal heatings of about 0.8°C were found for $U \approx 2$ m s^{-1}, which is two times less than the formulation given by Hasse (1971). A maximum diurnal heating of 5°C is found for nul wind conditions, which is in agreement with the value calculated from the radiative and heat transfer equation assuming the thermal diffusivity is only molecular.

TABLE 2. Relative frequencies of low wind speeds: N_1: nul; N_2: Beaufort forces 1 and 2 ($1 < U < 3$ m s^{-1}), during June, July and August in the French Mediterranean coastal area, (Darchen, 1974). An estimate of the mean diurnal heating $\bar{\Delta}T$ is given in column (3).

Station	N_1 (%)	N (%)	$\bar{\Delta}T$ (°C)
Cap Bear	16.0	26.9	0.67
Sète	9.5	42.3	0.66
Panègues	21.3	26.8	0.80
Cap Camarat	10.8	46.6	0.74
Cap Ferrat	35.1	50.4	1.38
Cap Corse	18.4	35.5	0.82
Pertusato	6.4	21.0	0.37
42°N–6°E	7.6	/	/

Acknowledgments. HCMR data have been received from NASA as a support to HCMR Investigation No. 15. Thanks to L. F. Martin for his aid in the translation. Support for this work has been provided by the following French agencies: CNRS (Centre National de la Recherche Scientifique) and CNES (Centre National d'Etudes Spatiales).

APPENDIX

Glitter Reflectance

Glitter refers to direct solar radiation reflected by the sea surface. This reflection is specular for a planar surface. When there is wind, the surface is agitated and consists of elements which are statistically distributed around the horizontal plane. This produces a more or less bright spot of variable dimensions which is commonly called glitter.

The radiance L_g reflected by the agitated sea surface can be expressed (Cox and Munk, 1956)

$$L_g = \frac{E_s}{4} \frac{R(\omega)}{\mu_v \mu_n^4} p, \tag{A1}$$

and the equivalent reflectance ρ_g will be expressed as

$$\rho_g = \frac{\pi L_g}{\mu_s E_s} = \frac{\pi}{4} \frac{R(\omega)}{\mu_s \mu_v \mu_n^4} p, \tag{A2}$$

where E_s is the direct solar radiation at sea level, $R(\omega)$ the reflection coefficient of water at a given incidence ω, p the probability of encountering a properly oriented surface element. In (A1) and (A2) $\mu_v = \cos\theta_v$, $\mu_s = \cos\theta_s$, $\mu_n = \cos\theta_n$, respectively, define the zenithal angles of the observation direction, the direction of incidence, and their bisector. One can deduce μ_n from the following equations:

$$\mu_n = \frac{\mu_s + \mu_v}{2 \cos\omega}, \tag{A3}$$

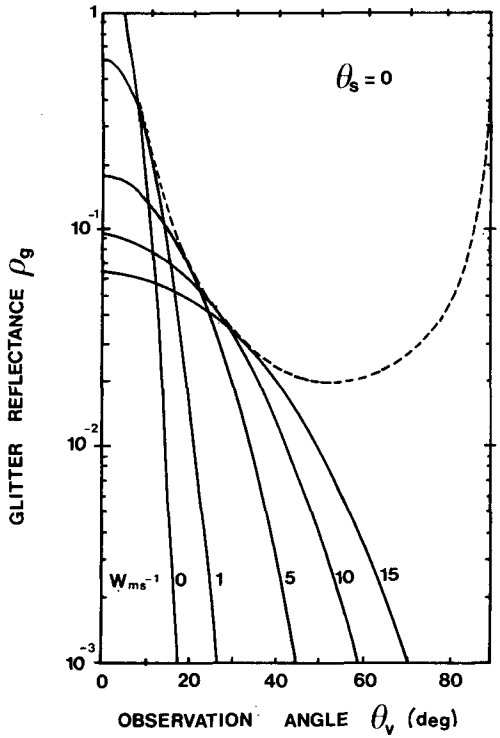

FIG. 6. Glitter reflectance vs zenithal viewing angle, for a sun at zenith, and several wind speeds from 0 to 15 m s^{-1}. Maximum glitter reflectance is given by a dashed line.

$$\cos 2\omega = \mu_s\mu_v + (1 - \mu_s^2)^{1/2}(1 - \mu_v^2)^{1/2}\cos\varphi, \quad \text{(A4)}$$

where φ is the relative azimuthal angle between the incidence and observation directions.

From a study of aerial photographs of glitter patterns, Cox and Munk (1956) developed p in a Gram–Charlier series which as a first approximation is reduced to a Gaussian distribution with revolution symmetry

$$p = \frac{1}{\pi\sigma^2}\exp\left[-\frac{(\tan\theta_n)^2}{\sigma^2}\right] \quad \text{(A5)}$$

with

$$\sigma^2 = 0.003 + 5.12 \times 10^{-3}U - 1 \pm 0.004 \quad \text{(A6)}$$

for $1 < U < 14$ m s^{-1}.

Figure 6 gives an example of the glitter spot ρ_g thus computed as a function of solar zenithal angle for different values of W, and for a nadir viewing ($\theta_v = 0$). In accordance with the reciprocity principle, by permutation (θ_s, θ_v), Fig. 6 also gives ρ_g as a function of the observation angle, for a sun at the zenith ($\theta_s = 0$). For a given angle ρ_g presents a maximum, ρ_{gm}, at a certain value of σ_m which is related to wind speed. The σ_m and ρ_{gm} are given by

$$\sigma_m^2 = \tan^2\theta_n = \mu_n^{-2} - 1, \quad \text{(A7)}$$

$$\rho_{gm} = \frac{R(\omega)}{4\mu_s\mu_v\mu_n^2(1 - \mu_n^2)}. \quad \text{(A8)}$$

The dashed curve in Fig. 6 envelops the preceding curves and represents the maximum glitter ρ_{gm} as defined by (A8).

REFERENCES

Cox, C. S., and W. H. Munk, 1954: Measurement of the roughness of the sea surface from photographs of the sun's glitter. *J. Opt. Soc. Amer.*, **44**, 838–850.

——, and ——, 1956: Slopes of the sea surface deduced from photographs of sun glitter. *Bull. Scripps Inst. Oceanogr.*, **6**, 401–488.

Darchen, J., 1974: Eléments climatologiques concernant les côtes de la France métropolitaine. *Monogr. No. 93, Météorologie Nationale* (77 rue de Sèvres, 92100 Boulogne Billancourt, France).

Hasse, L., 1971: The sea surface temperature deviation and the heat flow at the sea-air interface. *Bound.-Layer Meteor.*, **1**, 368–379.

Jerlov, N. G., 1968: *Optical Oceanography.* Elsevier, 194 pp.

Kraus, E. B., and J. S. Turner, 1967: A one-dimensional model of the seasonal thermocline. II: The general theory and its consequences. *Tellus*, **19**, 98–105.

La Violette, P. E., S. Peteherych and J. F. R. Gower, 1980: Oceanographic implications of features in NOAA satellite visible imagery. *Bound.-Layer Meteor.*, **18**, 159–175.

Pruvost, P., 1975: Etude du flux solaire et de l'échauffement radiatif dans la mer par temps clair. *Ann. Hydrogr.*, **3**, 25–34.

Roll, H. U., 1965: *Physics of the Marine Atmosphere.* Academic Press, 426 pp.

Romer, J., 1969: Variations de la température de surface de la mer au voisinage de la surface. *Note EERM No. 262, Météorologie Nationale* (77 rue de Sèvres, 92100 Boulogne Billancourt, France).

Simpson, J. J., and T. D. Dickey, 1981: The relationship between downward irradiance and upper ocean structure. *J. Phys. Oceanogr.*, **11**, 309–323.

Stommel, H., K. Saunders and J. Cooper, 1969: Observations of the diurnal thermocline. *Deep-Sea Res.*, **16** (Suppl), 269–284.